Journal of Zhejiang University-SCIENCE A (Applied Physics & Engineering)
ISSN 1673-565X (Print); ISSN 1862-1775 (Online)
www.jzus.zju.edu.cn; www.springerlink.com
E-mail: jzus@zju.edu.cn

Effect of cemented soil properties on the behavior of pre-bored grouted planted nodular piles under compression*

Jia-jin ZHOU[1,2], Xiao-nan GONG[†‡1,2], Kui-hua WANG[1,2], Ri-hong ZHANG[3], Guo-lin XU[3]

[1]*Research Center of Coastal and Urban Geotechnical Engineering, Zhejiang University, Hangzhou 310058, China*

[2]*MOE Key Laboratory of Soft Soils and Geoenvironmental Engineering, Zhejiang University, Hangzhou 310058, China*

[3]*ZCONE High-tech Pile Industry Holdings Co., Ltd., Ningbo 315000, China*

[†]E-mail: gongxn@zju.edu.cn

Received Mar. 6, 2017; Revision accepted Oct. 6, 2017; Crosschecked June 6, 2018

Abstract: A series of unconfined compressive strength tests of cemented soil and a model test of a pre-bored grouted planted nodular (PGPN) pile were conducted to investigate the effect of cemented soil properties on the behavior of PGPN piles under compression. The load-displacement response, axial force, and tip resistance were measured during the loading process. Several conclusions could be drawn by comparing the results of the present model test with those of a previous test: the compressive bearing capacity of the PGPN pile was enhanced by increasing the cemented soil strength; the ultimate skin friction of the PGPN pile was increased to 1.06–1.36 times when the strength of the cemented soil along the pile shaft increased from 0.706 MPa to 1.21 MPa; the ultimate mobilized base load was increased to 1.42 times when the strength of the cemented soil at the enlarged base increased from 11.10 MPa to 16.02 MPa.

Key words: Pre-bored grouted planted nodular (PGPN) pile; Cemented soil properties; Model test; Frictional capacity; Tip bearing capacity

https://doi.org/10.1631/jzus.A1700118 **CLC number:** TU473.1

1 Introduction

A pre-bored grouted planted nodular (PGPN) pile is a type of composite pile foundation consisting of a precast nodular pile and cemented soil around the pile shaft. There is an enlarged cemented soil base at the tip of a PGPN pile, which is effective in enhancing the tip bearing capacity. The compressive and uplift bearing capacities of a PGPN pile are better than that of a bored pile in soft soil areas (Zhou et al., 2013, 2015, 2017a, 2017b). The load transfer process of a PGPN pile is different from that of a conventional jacked or hammered prestressed high-strength concrete (PHC) pile or a cast in situ pile. The cemented soil along the precast pile shaft acts mainly as a transition layer in the load transfer process, and the cemented soil at the enlarged pile base supports part of the mobilized base load (Zhou et al., 2016).

The cemented soil plays an important role in the load transfer process of a PGPN pile, but no studies have been conducted to investigate the effect of cemented soil properties on the behavior of PGPN piles. This paper presents a model test of a PGPN pile. The effect of cemented soil properties on the behavior of the PGPN pile is investigated by comparing the results of the present model test with those of a previous test.

‡ Corresponding author

* Project supported by the National Natural Science Foundation of China (Nos. 51578498 and 51579217), the China Postdoctoral Science Foundation (No. 2017M611995), and the Science and Technology Plan Program of Ningbo, China (No. 2013B81003)

ORCID: Jia-jin ZHOU, https://orcid.org/0000-0003-4267-1454; Xiao-nan GONG, https://orcid.org/0000-0001-5218-5324

2 Model test preparation

To investigate the influence of cemented soil properties on the behavior of a PGPN pile, the model nodular pile, soil profiles, and properties in the present model test were all controlled to be identical to those in the previous model test. Hence, a 90 (60)-mm nodular pile (in which the diameter of the node on the pile is 90 mm and the diameter of the pile shaft is 60 mm) was used, and the distance between adjacent nodes was 200 mm. The entire length of the model pile was 2000 mm. The diameter of the cemented soil along the pile shaft was 110 mm. The diameter of the enlarged cemented soil base was 165 mm, and the height of the enlarged base was 330 mm. The scales of the nodular pile and the cemented soil were both identical to those in the previous model test (Zhou et al., 2016). Eight groups of strain gauges, set as full-bridge circuits, were attached to the nodular pile shaft to measure the axial load during a static load test. Three soil pressure sensors were equipped beneath the pile tip to measure the tip resistance. When fitting the strain gauges, abrasive paper was used to smooth the surface of the nodular pile, and anhydrous alcohol was painted on the smoothed spot to remove dust during the volatilization process. The strain gauges were then set in place, and covered with epoxy resin to protect them. The model nodular pile, layout of the strain gauges along the pile shaft, and a schematic of the model PGPN pile are shown in Fig. 1.

The model test was conducted in a test chamber of 1.8 m×1.8 m×2.5 m (Fig. 2). The diameter of the nodes along the model nodular pile was 90 mm (Fig. 1b). The distance between the nodular pile and the edge of the test chamber was 10 times the pile diameter, and so the boundary effect could be ignored in this research.

The foundation soil preparation process was similar to that used in the previous study (Zhou et al., 2016). Specifically, to produce a uniform layer, the foundation soil was filled layer by layer such that the thickness of each soil layer was 0.1 m after compaction. In the present model test, the dry density of the soil mass was used to control the amount of each soil layer, and the specific dry density was set as 1.50 kg/m^3 for clayey soil and 1.60 kg/m^3 for sandy soil. The homogeneity of the foundation soil was examined after each soil layer was compacted completely, and the densities of soil samples obtained from five different places were tested. The next soil

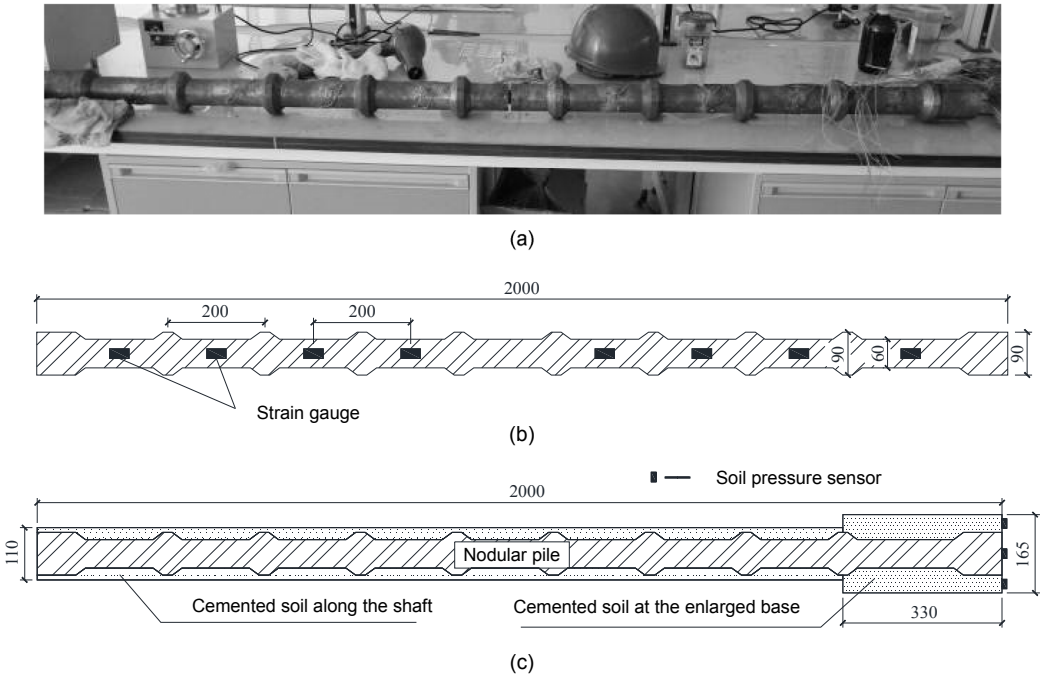

Fig. 1 Schematic of model pile and layout of strain gauges (unit: mm)
(a) Model nodular pile; (b) Layout of strain gauges; (c) Schematic of the PGPN pile

layer should not be added until the average density of the soil samples did not deviate by over 5% from the designed value.

Fig. 2 Photograph of the test chamber

Conventional geotechnical tests were carried out after each soil layer was compacted to the designed density. The soil profiles and properties are shown in Table 1.

To simulate the prototype PGPN pile in actual projects, a 110-mm diameter steel pipe was buried in advance in the foundation soil preparation process to maintain the space for the model PGPN pile. Also, the enlarged pile base (Fig. 1c) was constructed in advance. The steel pipe was pulled out after the foundation soil process was completed, and the cemented soil was then put into the pile hole. The installation process of the model PGPN pile was slightly different from that of prototype PGPN piles in actual projects, and the drilling and grouting process was not simulated in the model test. Nevertheless, the cemented soil mixture was stirred to ensure uniformity before being poured into the pile hole in the model test, and the model nodular pile was surrounded by homogeneous cemented soil. The stress release process existed in the model pile installation process when the steel pipe pile was pulled out from the foundation soil. The model PGPN pile can be considered to be nearly the same as a PGPN pile in actual projects.

3 Unconfined compressive strength test

Unconfined compressive strength tests were conducted to investigate the properties of the cemented soil with different 'cement:soil:water' ratios. The typical clayey soil found in Ningbo, China and P.O 52.5 cement were used to produce cemented soil. The soil was first dried in an oven and then pulverized. Finally, the soil was put through a 1-mm sieve, to guarantee that the clayey soil grains and cement grains could easily be stirred to be homogeneous. During the cemented soil manufacturing process, the cement and soil grains were first stirred to ensure uniformity, and then water was added to the mixture. The compositions of the six kinds of cemented soil with different 'cement:soil:water' ratios are shown in Table 2. The cemented soil samples were all in a liquid state because of the high water content.

The cemented soil samples were all made in 70.7 mm×70.7 mm×70.7 mm molds, according to the test approach used for cement mortar. The samples were then cured in a standard curing room for 28 d under a controlled temperature of (20±2) °C. The tests were conducted in a 10-kN universal testing machine. A displacement control method was adopted in the test, and the loading speed was 0.5 mm/min.

The test results are presented in Table 3. The relationship between the cement content and unconfined compressive strength is presented in Fig. 3. Table 3 shows that the unconfined compressive strength of the cemented soil increased with increasing cement content, regardless of the influence of the water content, which was limited in the range from 54.69% to 69.08%. Fig. 3 shows that the strength of

Table 1 Soil profiles and properties

Layer identifier	Soil layer	Thickness (m)	γ (kN/m^3)	φ (°)		c (kPa)	E_p (MPa)
				Peak strength	Residual strength		
1	Clayey soil	1.8	18.5	35.8	30.5	25.5	5.4
2	Sandy soil	0.7	20.0	38.0	34.5	0	16.0

γ: gravity of the soil mass; c: cohesion of the soil; φ: internal frictional angle of the soil; E_p: compression modulus of the soil

Table 2 Cemented soil proportions

Cemented soil	Water cement ratio (cement paste)	Volumetric ratio (cement paste:slurry)	m_{cement}:m_{water}:m_{soil}	Cement content (%)	Water content (%)
Along the shaft	1.0	0.3	1:3.71:5.41	10.97	57.80
	1.0	0.5	1:2.62:3.25	17.04	61.65
	1.0	1.0	1:1.18:1.62	29.15	69.08
At the enlarged base	0.6	1.0	1:1.17:1.13	43.53	54.69
	0.6	1.5	1:0.98:0.75	57.76	55.70
	0.6	2.0	1:0.88:0.57	69.03	56.39

Cement content=$m_{cement}/(m_{water}+m_{soil})$; water content=$m_{water}/(m_{cement}+m_{soil})$

Table 3 Results of the unconfined compressive strength tests

Cemented soil	Water cement ratio (cement paste)	Volumetric ratio (cement paste:slurry)	Water content (%)	Cement content (%)	q_s (MPa)
Along the shaft	1.0	0.3	57.80	10.97	1.21
	1.0	0.5	61.65	17.04	1.79
	1.0	1.0	69.08	29.15	3.51
At the enlarged base	0.6	1.0	54.69	43.53	10.23
	0.6	1.5	55.70	57.76	12.83
	0.6	2.0	56.39	69.03	16.02

q_s: average strength of the cemented soil samples

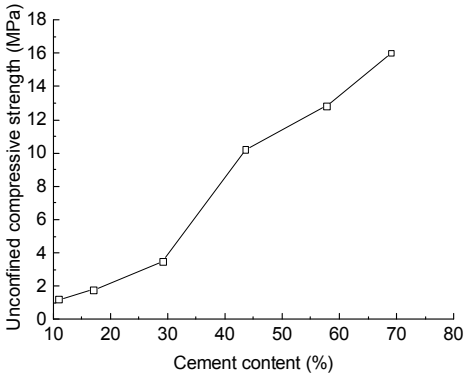

Fig. 3 Relationship between cement content and unconfined compressive strength

the cemented soil increased steadily from 1.21 MPa to 16.02 MPa when the cement content increased from 10.97% to 69.03%.

In the present model test, to investigate the influence of cemented soil properties on the behavior of the PGPN pile, the strength of the cemented soil along the shaft was 1.21 MPa, which was 1.71 times the strength of the cemented soil in the previous test (0.706 MPa). The strength of the cemented soil at the enlarged base was 16.02 MPa in the present test, 1.44 times the strength of the cemented soil in the previous test.

4 Static load test

A static load test was carried out after the cemented soil was cured for 28 d. The static load test was applied according to the local specification in China (MOHURD, 2014), and the slow maintained load method was adopted for the model test. The pile head load was applied by a 200-kN hydraulic jack, and the pile head displacement was measured by a dial indicator. A schematic of the model test is depicted in Fig. 4. During the loading process, the magnitude of each loading step was 5 kN, and the pile head settlement was measured at 5 min, 15 min, 30 min, etc., after each loading step until the settlement remained almost constant (in this model test, the settlement was always no greater than 0.1 mm within 1 h). According to the local specification (MOHURD, 2014), the static load test should terminate when the pile head displacement was larger than 40 mm.

5 Analysis of test results

5.1 Load-displacement response

The load-displacement responses of the two model tests are presented in Fig. 5, where TP1 and

TP2 represent the test piles in the previous and present model tests, respectively. The behavior of TP2 is obviously better than that of TP1.

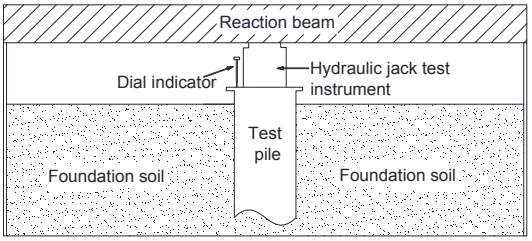

Fig. 4 Schematic of static load test

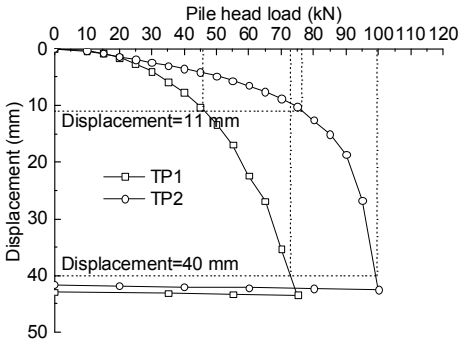

Fig. 5 Load-displacement curves of two test piles

According to Fleming et al. (2009), a pile was considered to have achieved its ultimate bearing capacity when the pile head displacement reaches $D/10$ (where D represents the pile diameter). The pile head load of TP1 was 46 kN when the pile head displacement reached 11 mm ($D/10$, where the diameter of cemented soil along the nodular pile shaft was taken as the model pile diameter), and the pile head load of TP2 was 76 kN when the pile head displacement was $D/10$. Hence, the pile head load of TP2 was 1.65 times the pile head load of TP1 when the pile head displacement reached $D/10$. The local specification (MOHURD, 2014) proposes that the bearing capacity of a pile foundation reaches the ultimate value when the pile head displacement is larger than 40 mm. The ultimate bearing capacities of the two test piles were therefore assumed to be 70 kN and 95 kN, respectively. Thus, the ultimate bearing capacity of TP2 was 1.36 times that of TP1.

As mentioned in Section 2, the soil properties and profiles of the two model tests were almost the same, and the behavior of the model pile was considered to be influenced mainly by the cemented soil properties. Hence, it can be considered that the ultimate compressive bearing capacity of the PGPN pile was increased to 1.36 times when the strength of the cemented soil along the shaft increased from 0.706 MPa to 1.21 MPa, and the strength of the cemented soil at the enlarged base increased from 11.10 MPa to 16.02 MPa.

5.2 Skin friction analysis

The axial force of the model PGPN pile under different loads was measured by the strain gauges fitted along the pile shaft, and the skin friction of the pile shaft in each soil layer could be calculated based on the axial force. The pile-soil relative displacement could be estimated only approximately using the following equation, as soil displacement data were lacking:

$$\delta_i = S - \sum_{j=1}^{i} \frac{L_j}{2}(\varepsilon_j + \varepsilon_{j+1}), \tag{1}$$

where δ_i is the displacement of pile shaft i (δ_i is taken as the approximate pile-soil relative displacement of pile shaft i), S is the pile head displacement, L_j is the length of pile shaft j, and ε_j and ε_{j+1} are the strains of pile shafts j and j+1, respectively.

The relationship between the skin friction and pile-soil relative displacement is presented in Fig. 6. The skin friction of each soil layer was gradually mobilized with increasing pile-soil relative displacement, and showed a small reduction after reaching the maximum value. The displacement needed to fully mobilize the skin friction was in the range of 6.5–8.8 mm, which was about 0.059D–0.08D (where D is the pile diameter).

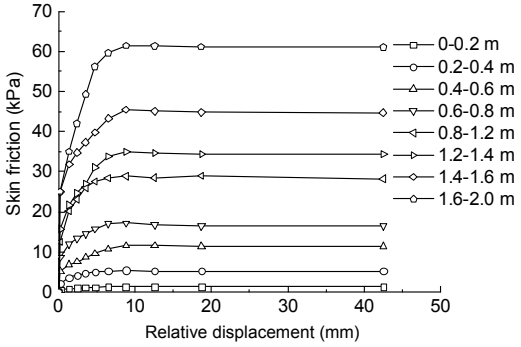

Fig. 6 Skin friction versus pile-soil relative displacement

To investigate the influence of the cemented soil strength on the frictional capacity of the PGPN pile, the ultimate skin frictions of each of the two model tests are compared in Table 4. For each soil layer, the ultimate skin friction of TP2 was larger than that of TP1, and the degree of increase was in the range of 1.06–1.36 fold. This range is fairly large, probably because the homogeneity of cemented soil, the permeation distance, and the permeability of the soil mass around the pile all affected the frictional capacity of the PGPN pile. Nevertheless, the results suggest that the ultimate skin friction of the PGPN pile was enhanced when the strength of the cemented soil along the shaft increased from 0.706 MPa to 1.21 MPa.

The shaft capacity of pile foundation has been investigated by many scholars (Kraft et al., 1981; Randolph and Wroth, 1981; Gavin and Lehane, 2003; Randolph, 2003; Doherty and Gavin, 2011). O'Neill (2001) pointed out that the frictional capacity of the pile-soil interface was influenced by many factors, such as the properties of the surrounding soil, pile foundation type, construction method, and pile shaft quality. In the two model tests, the properties of the surrounding soil were similar to each other, and the influence of the construction process could also be ignored. Therefore, the different ultimate skin frictions of the two model tests were probably induced by the different frictional angles of the pile-soil interface or the different pile-soil interface roughness coefficients R (Desai et al., 1985). As mentioned in Section 3, the cemented soil was in a liquid state, and a small amount of cemented soil would have permeated into the surrounding soil when being poured into the pile hole. The permeation of cemented soil can increase the roughness coefficient of the cemented soil-soil interface, and this effect would be greater in cemented soil with a larger strength.

To give a detailed comparison of the relationship between the skin friction and the pile-soil relative displacement of the test pile, a hyperbolic nonlinear model was used to investigate the effect of cemented soil properties on the frictional capacity of the PGPN pile. The relationship between the skin friction and pile-soil relative displacement can be expressed by the following equation:

$$p_s(z)=\frac{s(z)}{a+b\cdot s(z)}, \tag{2}$$

where $p_s(z)$ is the skin friction at depth z, $s(z)$ is the pile-soil relative displacement at depth z, and a and b are empirical coefficients that are always determined by back-analysis of the field test results. Randolph and Wroth (1978) proposed an equation to calculate the value of a:

$$a=\frac{r_0}{G_s}\ln\left(\frac{r_m}{r_0}\right), \tag{3}$$

$$r_m=2.5L(1-0.5\mu), \tag{4}$$

where r_0 is the radius of the pile shaft, G_s is the shearing modulus of the soil around the pile shaft, r_m is the distance from the pile center to the place where the shear stress induced by the pile can be ignored, L is the total length of the pile, and μ is Poisson's ratio of the soil around the pile shaft.

The value of b can be calculated by the following equation:

$$b=\frac{1}{p_{su}}=\frac{R_f}{p_u}, \tag{5}$$

where p_{su} is the ultimate skin friction, p_u is the maximum possible value of the skin friction, and R_f is the failure ratio. The values of R_f are commonly in the range of 0.80–0.95 (Clough and Duncan, 1971).

In the two model tests, the radius of the pile shaft r_0 was 55 mm, the entire length of the pile was 2 m, and the Poisson's ratio of the soil mass μ was 0.35. Comparisons between the measured and fitted results are presented in Fig. 7, and the values of the failure ratio R_f and the shearing modulus of the soil mass around the pile shaft are shown in Table 5. The

Table 4 Comparison of skin frictions of the two model tests

Soil layer depth (m)	Ultimate skin friction (kPa)	
	TP1	TP2
0–0.2	1.23	1.30
0.2–0.4	4.56	5.36
0.4–0.6	8.92	11.6
0.6–0.8	13.3	17.2
0.8–1.2	21.4	29.0
1.2–1.4	30.0	34.9
1.4–1.6	35.6	45.5
1.6–2.0	57.4	61.5

proposed hyperbolic model fits well with the measured results, which demonstrates the reliability of the fitted results (Fig. 7). Table 5 shows that the failure ratios (R_f) of the soil layers in the two tests were all 0.95, except for the 0–0.2 m soil layer for which the failure ratio was 1.00. The shearing modulus of the soil of TP2 was larger than that of TP1 for several soil layers.

5.3 Mobilized base load

The mobilized base load of the test pile was measured by the three soil pressure sensors fitted under the pile tip. The relationship between the mobilized base load and the tip displacement is presented in Fig. 8.

The entire mobilized base load of the PGPN pile consists of the tip resistances provided by the nodular pile and the enlarged cemented soil base. When the tip displacement was within 8.8 mm, the tip resistance provided by the nodular pile and the load provided by the enlarged cemented soil base both increased with increasing tip displacement. Nevertheless, the tip resistance provided by the enlarged cemented soil base remained nearly constant after the tip displacement reached 8.8 mm, while the tip resistance provided by the nodular pile continued to increase with increasing tip displacement.

The ratios of the mobilized base load provided by the nodular pile and the enlarged cemented soil base under different loads are presented in Fig. 9, where P_b is the entire mobilized base load, P_n is the tip resistance provided by the nodular pile, and P_c is the tip resistance provided by the enlarged cemented soil base. P_n and P_c were almost identical to each other when P_b was less than 22 kN, and the difference between P_n and P_c gradually increased with P_b being further mobilized. Specifically, the value of P_c remained almost constant after P_b reached 48 kN. Finally, the mobilized base load provided by the nodular pile, P_n, contributed 71.7% of the tip resistance, and the load provided by the cemented soil, P_c, contributed 28.3% of the entire tip resistance. This phenomenon is similar to that found in the previous test (Zhou et al., 2016). This is probably because the modulus of the cemented soil was much smaller than that of the precast nodular pile, thereby creating a larger strain in the cemented soil.

The mobilized base loads of the two test piles were also compared to investigate the effect of cemented soil properties on the tip bearing capacity of

Table 5 Values of R_f and shearing modulus of soil mass around the shaft

Soil layer depth (m)	R_f		G_s (MPa)	
	TP1	TP2	TP1	TP2
0–0.2	1.00	1.00	2.0	2.0
0.2–0.4	0.95	0.95	2.4	3.0
0.4–0.6	0.95	0.95	4.0	4.0
0.6–0.8	0.95	0.95	8.0	9.0
0.8–1.2	0.95	0.95	13.0	20.0
1.2–1.4	0.95	0.95	15.0	20.0
1.4–1.6	0.95	0.95	20.0	20.0
1.6–2.0	0.95	0.95	16.0	25.0

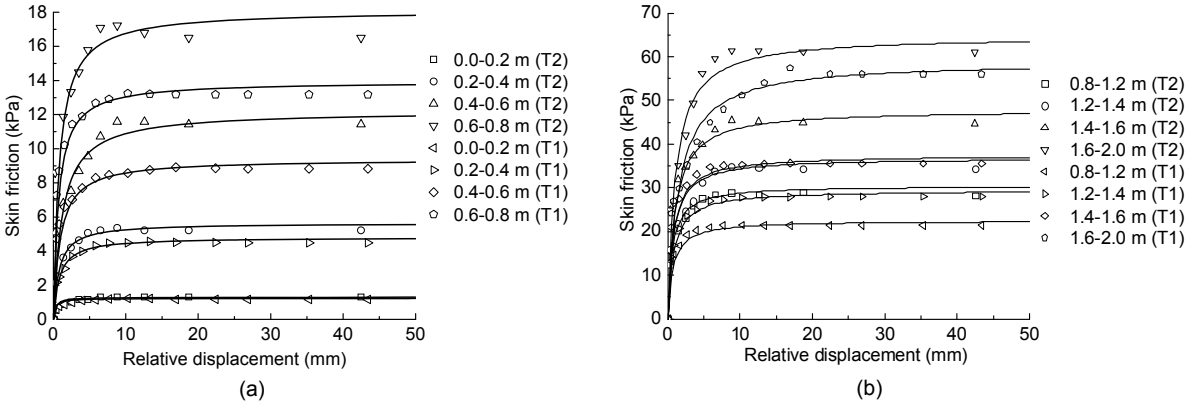

Fig. 7 Comparisons between measured and fitted results for the relationship between skin friction and relative displacement: (a) upper four soil layers; (b) lower four soil layers

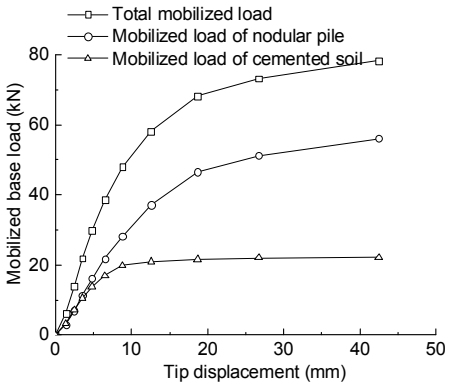

Fig. 8 Pile tip displacement versus mobilized base load

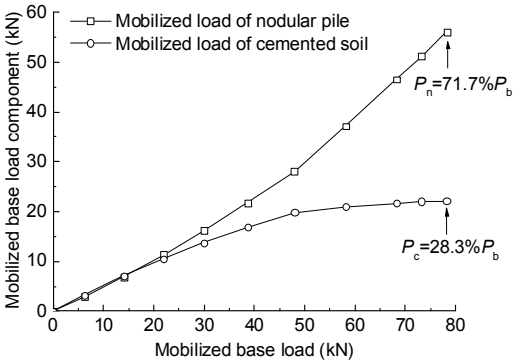

Fig. 9 Composition ratio of mobilized base load under different loads

the PGPN pile. The relationships between the mobilized base load and the tip displacement of the two model tests are presented in Fig. 10. The tip bearing capacity of TP2 was obviously better than that of TP1. Specifically, the ultimate mobilized base load of TP2 was 73.2 kN, which is 1.42 times the ultimate mobilized base load of TP1 (51.7 kN). Moreover, the tip displacement of TP2 was much smaller than that of TP1 under identical tip resistance. Therefore, it can be considered that the tip bearing capacity of the PGPN pile was largely improved when the strength of the cemented soil increased from 11.10 MPa to 16.02 MPa.

The pile tip settlement calculation has been extensively investigated by many scholars. Hyperbolic, exponential, power function, and bilinear models have been widely used to simulate pile tip behaviors (Poulos, 1968; Randolph and Wroth, 1979; Guo and Randolph, 1999; Lee and Xiao, 2001; Han and Ye, 2006). The tip load-displacement curves of the PGPN piles (Fig. 10) are nonlinear curves, and a nonlinear model is considered to be more suitable for simulating the tip behavior of a PGPN pile. Randolph and Wroth (1978) proposed an empirical equation to calculate pile tip displacement:

$$S_b = \frac{P_b(1-\mu)}{4r_b G_b}, \tag{6}$$

where S_b is the pile tip displacement, μ is Poisson's ratio of the soil mass under the pile tip, G_b is the shearing modulus of the soil mass under the pile tip, and r_b is the radius of the pile tip. Poisson's ratio of the soil mass under the pile tip was 0.3, and the radius of the pile tip was 82.5 mm.

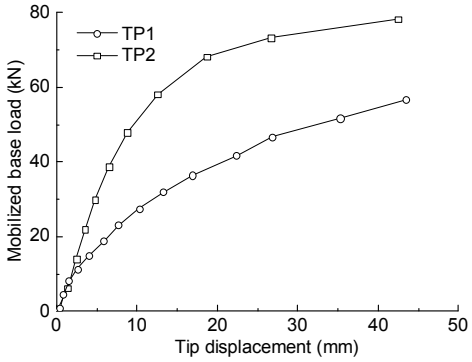

Fig. 10 Mobilized base load versus tip displacement curves of two model tests

Fig. 10 also shows that the shearing modulus of the tip load-displacement curve decreased with increasing tip displacement. This was due to the degradation of the shearing modulus of the base soil layer. Han and Ye (2006) proposed an empirical equation to simulate the degradation of the shearing modulus:

$$G_b = G_{b0}\left(1 - R_f \frac{P_b}{Q_b}\right)^2, \tag{7}$$

where G_{b0} is the initial shearing modulus of the soil under the pile tip and Q_b is the ultimate tip bearing capacity. The initial shearing modulus of the soil mass can be calculated by referring to the initial section of the tip load-displacement curve. The calculated shearing moduli of the soil mass were 11.5 MPa and 21.2 MPa for TP1 and TP2, respectively. The properties of the foundation soil of TP1 and TP2 were

almost identical to each other, and the initial shearing modulus of the soil mass for TP2 was higher because the strength of the cemented soil poured into the pile tip had increased from 11.10 MPa to 16.02 MPa. The simulation curves of the tip load-displacement responses of the two model tests are presented in Fig. 11. For TP1, the simulation curve fits the measured results well when the failure ratio was 0.55 or 0.60; while for TP2, the simulation curve fits the measured results well when the failure ratio was 0.45. Hence, it can be considered that the conventional nonlinear model can represent the tip load-displacement response of the PGPN pile when considering the precast nodular pile tip and the enlarged cemented soil base as a whole.

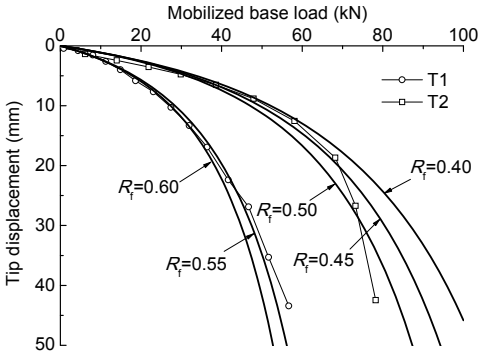

Fig. 11 Simulation curves of tip displacement versus mobilized base load

6 Conclusions

In this paper, a series of unconfined compressive strength tests of cemented soil and a model test were carried out to investigate the effect of cemented soil properties on the behavior of a PGPN pile under compression. Based on the test results presented, the following conclusions can be drawn:

1. For typical Ningbo clayey soil, the cemented soil strength increased steadily with increasing cement content, increasing from 1.21 MPa to 16.02 MPa when the cement content increased from 10.97% to 69.03%.

2. The behavior of the PGPN pile was enhanced by increasing cemented soil strength, and the ultimate compressive bearing capacity of the PGPN pile increased by 36% when the strength of the cemented soil along the shaft increased from 0.706 MPa to 1.21 MPa, and the strength of the cemented soil at the pile base increased from 11.10 MPa to 16.02 MPa.

3. The ultimate skin friction of the PGPN pile increased to 1.06–1.36 times when the strength of the cemented soil along the pile shaft increased from 0.706 MPa to 1.21 MPa, and the shearing modulus of the soil around the pile also increased in several soil layers. The frictional capacity of a PGPN pile is influenced by many factors, and much more work is needed to give a detailed analysis.

4. The ultimate tip bearing capacity of the PGPN pile increased to 1.42 times when the strength of the cemented soil at the enlarged base increased from 11.10 MPa to 16.02 MPa. The conventional nonlinear model can represent the tip load-displacement response of the PGPN pile well when taking the precast nodular pile tip and the enlarged cemented soil base as a whole.

5. For the application of the PGPN pile in practical projects, increasing the strength of the cemented soil at the enlarged pile base can improve the tip bearing capacity of the PGPN pile; the influence of the cemented soil strength along the pile shaft on the frictional capacity of the PGPN pile was not significant considering the relative large range of variation in the magnitude of the effect. More work is needed to obtain the proper value of cemented soil strength in different soil layers.

References

Clough GW, Duncan JM, 1971. Finite element analysis of retaining wall behavior. *ASCE Soil Mechanics & Foundation Division Journal*, 97(12):1657-1673.

Desai CS, Drumm EC, Zaman MM, 1985. Cyclic testing and modeling of interfaces. *Journal of Geotechnical Engineering*, 111(6):793-815. https://doi.org/10.1061/(ASCE)0733-9410(1985)111:6(793)

Doherty P, Gavin K, 2011. Shaft capacity of open-ended piles in clay. *Journal of Geotechnical & Geoenvironmental Engineering*, 137(11):1090-1102. https://doi.org/10.1061/(ASCE)GT.1943-5606.0000528

Fleming K, Weltman A, Randolph M, et al., 2009. Piling Engineering (3rd Edition), Taylor & Francis, London, UK.

Gavin K, Lehane B, 2003. The shaft capacity of pipe piles in sand. *Canadian Geotechnical Journal*, 40(1):36-45. https://doi.org/10.1139/t02-093

Guo WD, Randolph MF, 1999. An efficient approach for settlement prediction of pile groups. *Geotechnique*, 49(2):161-179. https://doi.org/10.1680/geot.1999.49.2.161

Han J, Ye SL, 2006. A field study on the behavior of micropiles in clay under compression or tension. *Canadian Geotechnical Journal*, 43(1):19-29. https://doi.org/10.1139/t05-089

MOHURD (Ministry of Housing and Urban-Rural Development of People's Republic of China), 2014. Building Pile Testing Technology Code, JGJ 106-2014. MOHURD, Beijing, China (in Chinese).

Kraft LMJ, Ray RP, Kakaaki T, 1981. Theoretical T-Z curves. *Journal of the Geotechnical Engineering Division*, 107(11):1543-1561.

Lee KM, Xiao ZR, 2001. A simplified nonlinear approach for pile group settlement analysis in multilayered soils. *Canadian Geotechnical Journal*, 38(5):1063-1080. https://doi.org/10.1139/t01-034

O'Neill MW, 2001. Side resistance in piles and drilled shafts. *Journal of Geotechnical & Geoenvironmental Engineering*, 127(1):3-16. https://doi.org/10.1061/(ASCE)1090-0241(2001)127:1(3)

Poulos HG, 1968. Analysis of the settlement of pile groups. *Geotechnique*, 18(4):449-471. https://doi.org/10.1680/geot.1968.18.4.449

Randolph MF, 2003. Science and empiricism in pile foundation design. *Geotechnique*, 53(10):847-875. https://doi.org/10.1680/geot.2003.53.10.847

Randolph MF, Wroth CP, 1978. Analysis of deformation of vertically loaded pile. *Journal of the Geotechnical Engineering Division*, 104(12):1465-1488.

Randolph MF, Wroth CP, 1979. An analysis of the vertical deformation of pile groups. *Geotechnique*, 29(4):423-439. https://doi.org/10.1680/geot.1979.29.4.423

Randolph MF, Wroth CP, 1981. Application of the failure state in undrained simple shear to the shaft capacity of driven piles. *Geotechnique*, 31(1):143-157. https://doi.org/10.1680/geot.1981.31.1.143

Zhou JJ, Wang KH, Gong XN, et al., 2013. Bearing capacity and load transfer mechanism of a static drill rooted nodular pile in soft soil areas. *Journal of Zhejiang University-SCIENCE A (Applied Physics & Engineering)*, 14(10):705-719. https://doi.org/10.1631/jzus.A1300139

Zhou JJ, Gong XN, Wang KH, et al., 2015. A field study on the behavior of static drill rooted nodular piles with caps under compression. *Journal of Zhejiang University-SCIENCE A (Applied Physics & Engineering)*, 16(12):951-963. https://doi.org/10.1631/jzus.A1500168

Zhou JJ, Wang KH, Gong XN, et al., 2016. A model test on the behavior of a static drill rooted nodular pile under compression. *Marine Georesources & Geotechnology*, 34(3):293-301. https://doi.org/10.1080/1064119X.2015.1012313

Zhou JJ, Gong XN, Wang KH, et al., 2017a. A simplified nonlinear calculation method to describe the settlement of pre-bored grouting planted nodular piles. *Journal of Zhejiang University-SCIENCE A (Applied Physics & Engineering)*, 18(11):895-909. https://doi.org/10.1631/jzus.A1600640

Zhou JJ, Gong XN, Wang KH, et al., 2017b. Testing and modelling the behavior of pre-bored grouting planted nodular pile under compression and tension. *Acta Geotechnica*, 12(5):1061-1075. https://doi.org/10.1007/s11440-017-0540-6

中文概要

题　目：水泥土性质对静钻根植竹节桩抗压承载性能影响

目　的：静钻根植竹节桩是一种由预制竹节桩和水泥土组成的组合桩基。通过一系列水泥土试块的无侧限抗压强度试验和静钻根植竹节桩的单桩模型试验，研究水泥土性质对静钻根植竹节桩抗压承载性能的影响。得出水泥土强度的提高对静钻根植竹节桩桩侧和桩端承载性能的影响规律，为静钻根植竹节桩的设计和推广应用提供理论依据。

创新点：1. 得出静钻根植竹节桩桩端扩大头中水泥土强度的提高对其桩端承载性能的影响规律；2. 得到静钻根植竹节桩桩周水泥土强度的提高对其桩侧摩擦性能的影响规律。

方　法：1. 通过改变静钻根植竹节桩桩端扩大头的水泥土强度的模型试验，得到桩端水泥土强度的提高对桩基桩端承载性能的影响规律；2. 通过桩周水泥土强度不同的静钻根植竹节桩的模型试验，得出静钻根植竹节桩桩周水泥土强度的提高对其桩侧摩擦性能的影响规律。

结　论：1. 提高水泥土强度能够改善静钻根植竹节桩的抗压承载性能；当桩周水泥土强度从0.706 MPa增加到1.21 MPa，桩端水泥土强度从11.10 MPa增加到16.02 MPa时，静钻根植竹节桩极限抗压承载力提高了36%。2. 当桩周水泥土强度从0.706 MPa增加到1.21 MPa时，不同深度土层中桩侧极限摩阻力增加到1.06–1.36倍。3. 桩端水泥土强度从11.10 MPa增加到16.02 MPa时，静钻根植竹节桩的极限桩端承载力增加到1.42倍。4. 在静钻根植竹节桩的实际工程应用中，增加桩端扩大头处水泥土强度能够有效提高桩基的承载性能，而桩周水泥土强度的增加对桩基侧摩阻力的提高效果不明显。

关键字：静钻根植竹节桩；水泥土性质；模型试验；摩擦性能；桩端承载性能